J. Fluid Mech. (1992), *vol.* 235, *pp.* 223–254
Printed in Great Britain

Instability mode interactions in a spatially developing plane wake

By HIROSHI MAEKAWA[1]†, NAGI N. MANSOUR[2] AND JEFFREY C. BUELL[2]

[1] Department of Mechanical Engineering, Kagoshima University, Kagoshima 890, Japan
[2] NASA Ames Research Center, Moffett Field, CA 94035, USA

(Received 14 February 1990 and in revised form 19 June 1991)

The transition mechanism in a spatially developing two-dimensional wake is studied by means of direct numerical simulations. Five different types of forcing of the inlet are investigated: fundamental mode, fundamental and one or two subharmonics, fundamental mode and random noise, and random noise only. The effects of the amplitude levels of the perturbations on the development of the layer are also investigated. Statistical analyses are performed and some numerical results are compared with experimental measurements. When only a fundamental mode is forced, the energy spectra show amplification of the fundamental frequency and its higher harmonics, and the development of a stable vortex street. When the inlet flow is forced by a fundamental mode and two subharmonics, a vortex street also appears downstream, but the shape of the vortices is distorted. The amplitude of the subharmonic grows only after the saturation of the fundamental. Amplification of modes close to the fundamental mode is observed when random noise of large amplitude is added to the fundamental mode. The phase jitter around the fundamental frequency plays a critical role in generating vortices of random shape and spacing. Large- and small-scale distortions of the flow structure are observed. Pairing of vortices of the same sign is observed, as well as coupling of vortices of opposite sign. When the inlet profile is forced by random noise of amplitude 10^{-5} times the free-stream velocity, one frequency close to the most unstable one is amplified more than the others. The energy spectrum is otherwise full. When the same low amplitude (10^{-5}) is used to force the fundamental mode and its two subharmonics, bands of energy develop around the forced modes and their harmonics. Finally, we find that large-deficit wakes are globally unstable when the size of the absolutely unstable region is greater than about three times the half-width of the wake

1. Introduction

In the past three decades, linear stability analysis (Sato & Kuriki 1961; Mattingly & Criminale 1972; Papageorgiou & Smith 1989) has led to a comprehensive understanding of the linear stage of transition in plane wakes. Our understanding of the nonlinear and turbulent stages is less well developed. Nonlinear theory developed by Papageorgiou & Smith (1988) using an asymptotic solution was used to study the long-wavelength regime in a wake. The nonlinear stages have been investigated experimentally, and a few numerical studies have examined the early nonlinear stages of forced wakes.

† Present address: Department of Mechanical and Control Engineering, University of Electro-Communications, Chofu, Tokyo I82, Japan.

Experimental studies of the wake have been carried out extensively by Sato & Kuriki (1961), Sato & Onda (1970), Sato & Saito (1975, 1978) and Gharib & Williams-Stuber (1989). Detailed measurements were made in the laminar-turbulent transition region of plane wakes with natural and various kinds of forced disturbances. In all cases, the transition to turbulence was gradual. Sato & Onda (1970) reported that the wake responds differently under different kinds of forcing. They find that the transition process strongly depends on the initial disturbance. In the nonlinear region, they reported the generation of velocity fluctuations at the harmonics of the forced frequencies. They conjectured that the slow and irregular fluctuations found in the natural transition might be the result of a nonlinear process of subtraction of two frequencies. They explained the experimental results by two empirical properties of the nonlinear interaction: the growth suppression induced by a large-amplitude fluctuations; and the strong interaction between fluctuations of similar amplitudes. Gharib & Williams-Stuber (1989) investigated the enhancement and cancellation of perturbations in a plane wake by the strip heater technique. They showed that the mean velocity profile adjusts itself to become more receptive to the forced frequency.

In their numerical study, Zabusky & Deem (1971) simulated temporally developing wakes with a single excited eigenmode as an initial condition using a finite-difference method. They showed the existence of a double row of elliptical vortices, and studied the behaviour of the spatial harmonics. They did not study the interactions of a fundamental with its subharmonics. Aref & Siggia (1981) used a vortex method to study a plane temporally developing wake defined by two vortex sheets. They showed that doublets, triplets and natural pairs form in a two-dimensional randomly forced wake. They also found that the asymptotic structure was highly dependent on initial conditions, and questioned the idea of universality of the far wake. Comte, Lesieur & Chollet (1989) studied the temporal wake using the Navier–Stokes equations. They computed the development of instabilities for both the forced case and the natural (random initial perturbation) case. They found doublets and pairings consistent with the results of Aref & Siggia (1981). Hannemann & Oertel (1989) simulated the wake behind a flat plate with a thick trailing edge using a finite-difference method. They also analysed the wake using stability analysis and found regions of local absolute and convective instability. An early theoretical investigation of the wake by Koch (1985) found absolute and convective instability regimes. The temporal amplification process of perturbations at supercritical Reynolds numbers was studied by Hultgren & Aggarwal (1987). They calculated the critical defect value and supercritical Reynolds numbers of absolutely unstable Gaussian wakes using nonlinear stability theory.

Many features of the experimental observations on forced wakes were reproduced by the numerical studies of temporally evolving layers. However, the effects on the layer development of random perturbations that occur naturally in an experiment were not considered in the numerical studies. In addition, a simulation that considers the spatially developing problem will more closely mimic the near-wake experiments.

The purpose of this investigation is to present numerical results for the spatial evolution of various instability modes. The interaction of these modes and the flow dynamics that are crucial to the understanding of the evolving structures in the transition region of the flow are investigated. The nonlinear interaction of instability modes and the growth of randomness are studied by means of statistical analysis and visualizations of the vorticity field. The effect of interaction of these modes on the flow structure is investigated. Finally, a quantitative measure of the size of the absolutely unstable region for global instability is found.

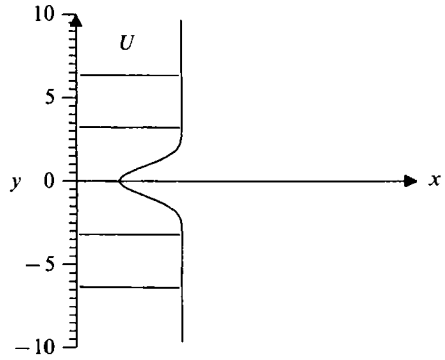

FIGURE 1. Coordinate system, with inlet Gaussian profile.

2. Mathematical formulation

2.1. *Governing equations*

The computational domain starts downstream of the trailing edge of a splitter plate. Figure 1 illustrates the computational domain and the coordinate system used. The streamwise (x) extent of the computational domain is finite, and the cross-stream (y) extent is infinite in both the positive and negative directions. The time-dependent incompressible Navier–Stokes equations are written in rotational form as follows:

$$\frac{\partial u_i}{\partial t} = \epsilon_{ijk} u_j \omega_k - \frac{\partial P}{\partial x_i} + \frac{1}{Re}\nabla^2 u_i, \quad i = 1, 2, \tag{1}$$

where P is the dynamic pressure, $Re = U_\infty b_{\frac{1}{2}}/\nu$ is the Reynolds number, $b_{\frac{1}{2}}$ is the half-width of the inlet Gaussian wake profile, and U_∞ is the free-stream velocity. Conservation of mass for the fluid is given by the continuity equation

$$\frac{\partial u_i}{\partial x_i} = 0. \tag{2}$$

All quantities are non-dimensionalized by the appropriate characteristic scales, U_∞ and $b_{\frac{1}{2}}$.

2.2. *Boundary conditions*

A Gaussian profile was chosen for the inlet velocity,

$$U(y) = 1 - 0.692 \exp\,(1 - 0.69315 y^2), \tag{3}$$

where the coefficient 0.692 in (3) is such that the centreline deficit will correspond to the experiment by Sato & Kuriki (1961). In the study of a large-deficit wake, this coefficient is set to 0.99. The coefficient 0.69315 produces a half-width of one. In addition to the mean flow, the inlet flow is forced with unstable eigenfunctions of the Orr–Sommerfeld equation for the Gaussian profile. Various linear combinations of the fundamental mode, first and second subharmonics are superimposed on the mean velocity at the inlet plane. These perturbations are of the form

$$u_j^{\mathrm{p}}(y, t) = \tfrac{1}{2}[\tilde{u}_j(y)\, \mathrm{e}^{\mathrm{i}\omega_{\mathrm{p}} t} + \mathrm{c.c.}], \tag{4}$$

where ω_{p} represents the frequency of oscillation of the eigenfunctions, and c.c. denotes complex conjugate. The random noise is created using the profiles of the eigenfunctions and random frequencies. This perturbation is of the form

$$u_j^{\mathrm{rp}}(y, t) = \tfrac{1}{2}[\tilde{u}_j(y)\, \mathrm{e}^{\mathrm{i}\omega_{\mathrm{rp}} t} + \mathrm{c.c.}], \tag{5}$$

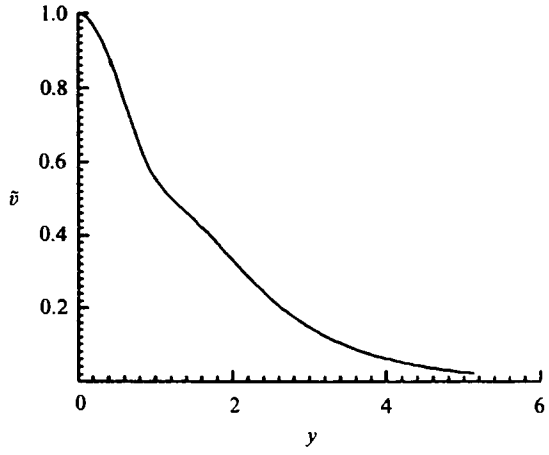

FIGURE 2. Profile of the forced fundamental eigenfunction.

where ω_{rp} is a random frequency generated by a random function. In this work, only the v-component was used to perturb the inlet flow. Figure 2 shows the profile of the fundamental eigenfunction, $\tilde{v}$, at $\omega = 0.608$ for the Gaussian wake represented by (3) at $Re = 600$.

A time-dependent advection condition of the form

$$\frac{\partial u_i}{\partial t} + U_a \frac{\partial u_i}{\partial x} = 0, \tag{6}$$

where U_a represents the advection speed of the large-scale structures in the layer, is applied to each of the velocity components at the exit plane. In addition to being fairly 'soft', this condition has the advantage of automatically satisfying global conservation of mass, as opposed to conditions that use a non-constant U_a or higher derivatives. This approach has been taken in other simulations of spatially developing free shear layers (see Davis & Moore 1985). The choice of $U_a = 1$ is most appropriate for simulations of small-deficit wakes, but we found that it is also appropriate for moderate-deficit wakes. We use a large computational domain in the x-direction, so the wake deficit is small in the exit plane.

The velocity components are split into computational variables and 'reference' profiles,

$$u = u_c(x, y, t) + U(y), \quad v = v_c(x, y, t), \tag{7}$$

where the computational variable are denoted by subscript c. This decomposition implies that the boundary conditions at infinity on the computational variables are homogeneous Dirichlet.

2.3. *Initial conditions*

The Gaussian profile prescribed for the mean u-component at the inlet plane is distributed uniformly at all x-locations in the domain at $t = 0$. These initial conditions must be allowed to 'wash out' before any statistical analysis can be performed on the solution. Laminar flow profiles calculated with no forcing at the inlet plane are used as the initial conditions to simulate the large-deficit wake.

3. Numerical method

The two-dimensional Navier–Stokes equations are solved on a domain that is infinite in the y-direction and finite in the x-direction. Pressure is eliminated by taking the curl of (1) twice. This yields a fourth-order equation for the streamwise velocity u:

$$\frac{\partial \nabla^2 u}{\partial t} = -\frac{\partial}{\partial y}\left(\frac{\partial H_1}{\partial y} - \frac{\partial H_2}{\partial x}\right) + \frac{1}{Re}\nabla^4 u, \tag{8}$$

where $H_i (i = 1, 2)$ represents the advection terms in the x- and y-momentum equations.

Equation (8) is advanced in time explicitly using a compact third-order Runge–Kutta scheme (Wray 1991). Since the Laplacian is contained in the time-derivative term, a Poisson equation must be solved during each substep. The cross-stream velocity v is recovered directly from the continuity equation. The algorithm is based on a Fourier method with a cotangent mapping in the y-direction ($y = -\beta \cot(\pi\zeta)$, with $\beta = 8$ for all of the present simulations), and fourth- and sixth-order accurate Padé finite-difference approximations (Lele 1991) in the x-direction. The algorithm contains no numerical diffusion, which we believe is important for problems where the dynamics are important. Furthermore, without numerical diffusion, marginal resolution in the x-direction will appear as high-wavenumber oscillations caused by dispersion, and is thus easily detected. In the y-direction, the Fourier coefficients always decayed by at least three to four orders of magnitude. Appropriate numbers of Fourier modes and grid points were determined after numerical tests on the resolution in both x- and y-directions at various Reynolds numbers (see § 4.1). For more details on the numerical scheme, the reader is referred to Buell (1991).

4. Vortical structure in a plane wake

4.1. *Summary of the numerical simulations*

Five cases were studied in the present work: Case 1 is a wake flow forced with a fundamental mode only; Case 2 is forced with a fundamental mode and its first subharmonic; Case 3 is forced with a fundamental mode and its first and second subharmonics; Case 4 is forced with the fundamental mode and random-phase noise In this case, the amplitudes of the fundamental mode and random-phase noise were 0.01 and 0.0005 (recall that all velocity amplitudes have been scaled with the free-stream velocity U_∞). Case 5 is forced with a random-phase noise only. In Cases 1 and 2, the amplitudes of the perturbations are 0.01. In Cases 3 and 5, the amplitudes are 0.00001 and 0.01. The Reynolds number ranged from 200 to 700. The simulation at $Re = 200$ used 384 uniformly distributed grid points in the x-direction over $0 \leqslant x \leqslant 200$, and 64 Fourier modes in the y-direction. At $Re = 300$, 512 grid points were used in the x-direction and 128 modes in the y-direction. At $Re = 600$, 768 grid points were used in the x-direction and 128 modes in the y-direction. For the large-deficit wake, 1536 grid points were used in the x-direction ($0 \leqslant x \leqslant 300$), and 128 modes in the y-direction. In this case the flow was forced with a fundamental of amplitude 0.0005 for only one period.

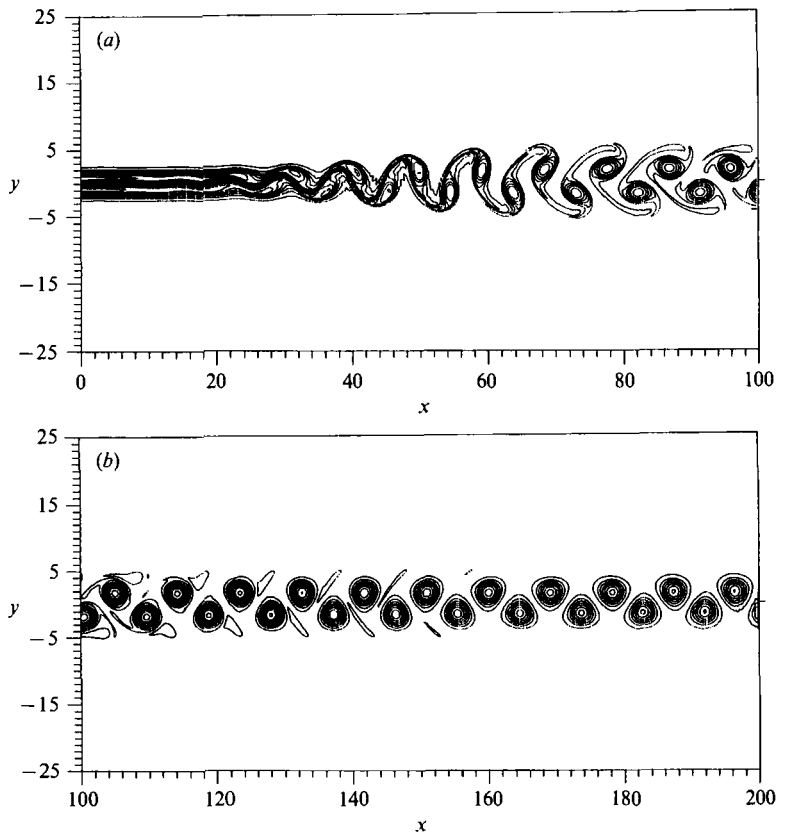

FIGURE 3. Vorticity contours; Case 1 at $Re = 600$ (contour interval: 0.0625 in (*a*), 0.045 in (*b*)).

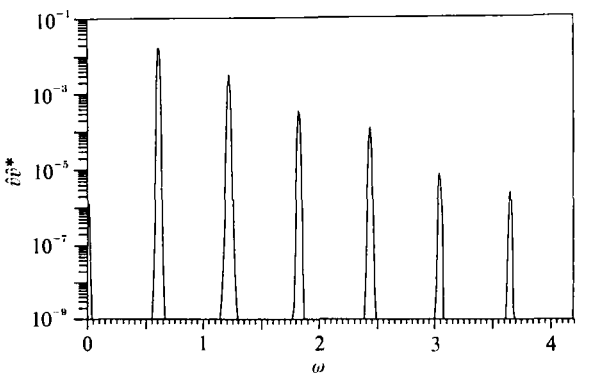

FIGURE 4. Energy spectrum of v; Case 1 at $Re = 600$ ($x = 50$, $y = 2.1$). Fundamental frequency is at $\omega = 0.608$.

4.2. *Generation of vortical structures*

Figure 3 shows vorticity contour plots for Case 1 at $Re = 600$. A street of alternate-signed vortices can be observed as the wake develops. Before the appearance of these vortices, the vorticity contour lines of the laminar wake begin to oscillate downstream of the inlet plane. After formation of the street, the vorticity is convected downstream with little further dynamics. In this case, the velocity fluctuations are

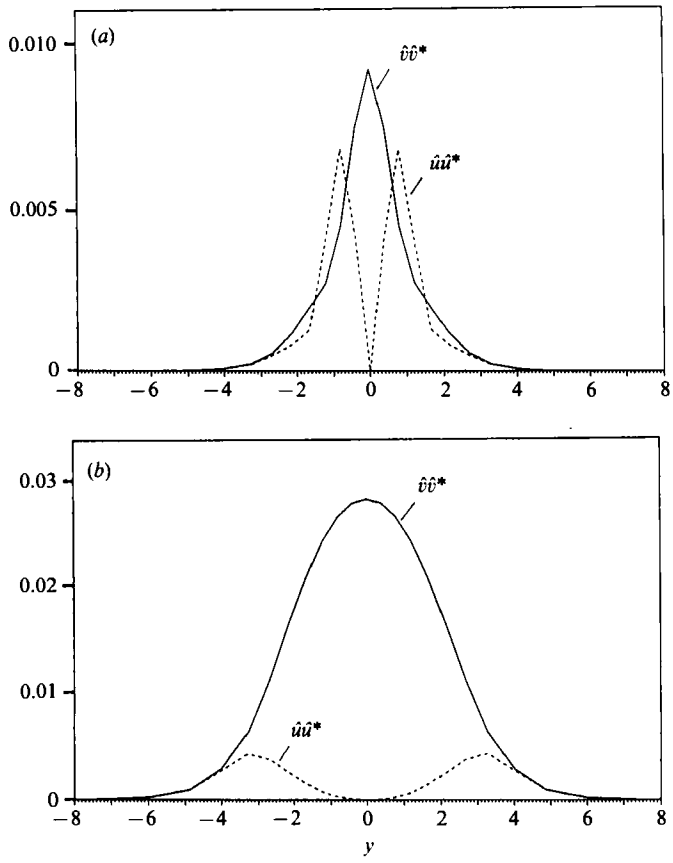

FIGURE 5. Profile of the fundamental mode ($\hat{v}\hat{v}^*$, $\hat{u}\hat{u}^*$); Case 1 at $Re = 600$. (*a*) $x = 25$ (*b*) $x = 50$.

periodic. Sharp peaks at the fundamental frequency and its higher harmonics in the energy spectrum of the v-signal can be seen in figure 4. Figures 5(*a*) and 5(*b*) show the cross-steam distributions of the velocity at the fundamental frequency, at $x = 25$ and 50, respectively. We notice that u has two peaks located approximately at the half-width of the layer while v has one peak at the wake centre. The fundamental mode grows rapidly downstream of the inlet plane. These results show that the spatial evolution of the fundamental mode is responsible for the generation of the vortex street.

In Case 3, with $Re = 200$ and a perturbation amplitude of 0.01, we find that the vortex street (figure 6) is significantly distorted compared to figure 3 by the presence of the subharmonic. The time traces of velocities are still periodic, but different from those of Case 1. The spectrum in this case (figure 7) still shows discrete frequencies. The fundamental frequency component and its two subharmonics can be detected, as well as their higher harmonics. The deformation of the vortex street is due to the spatial evolution of the subharmonic, which is discussed in §6.

In Case 5 (random-phase noise with amplitude equal to 0.00001), a clear vortex street is generated as the wake develops and the energy spectrum has a peak at the fundamental frequency. The profiles of the fundamental component (figure 8) and the vortical structures are similar to those of Case 1, but the magnitudes are smaller. On the other hand, when the amplitude of the random noise is 0.01, the vortical

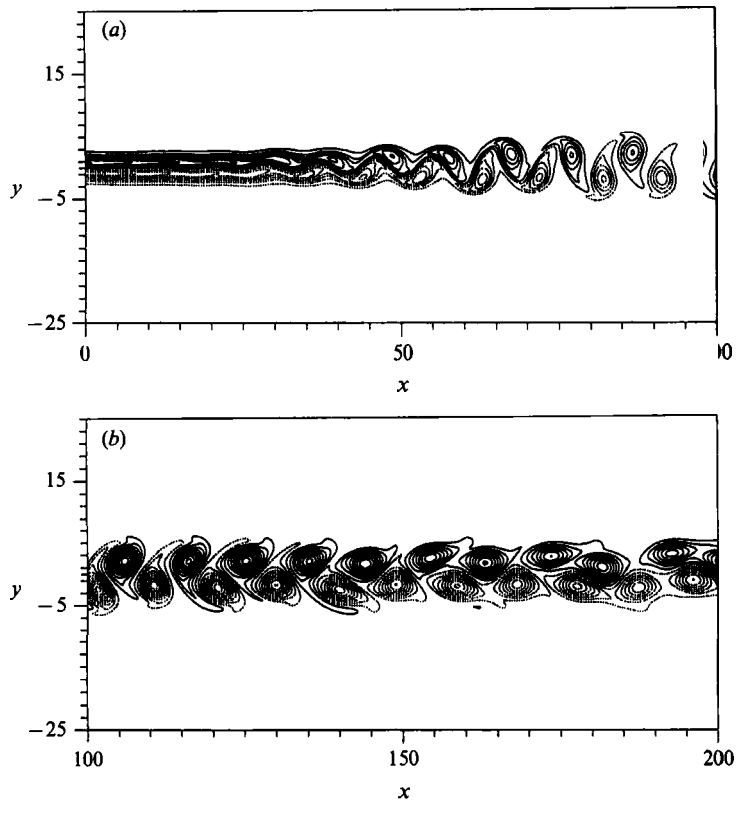

FIGURE 6. Vorticity contours; Case 3 at $Re = 200$ (contour interval: 0.05 in (a), 0.022 in (b)).

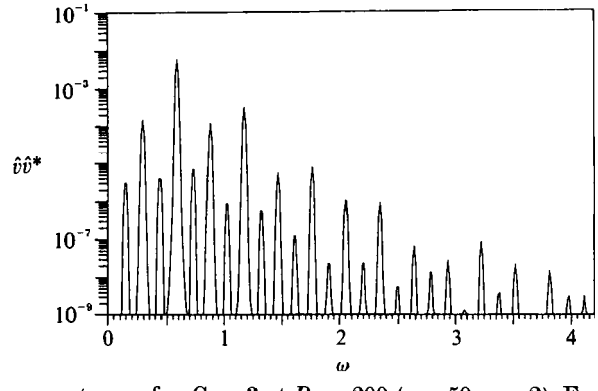

FIGURE 7. Energy spectrum of v; Case 3 at $Re = 200$ ($x = 50$, $y = 2$). Fundamental frequency is at $\omega = 0.586$. First and second subharmonic frequencies are at $\omega = 0.295$ and 0.147 respectively.

structure becomes non-periodic, as shown in figure 9. We observe an irregular configuration of vortices $x = 40$. This irregular configuration causes a large deformation of the vortex street. Figures 10(a) and 10(b) show the spectra for this case at the inlet plane and at $x = 25$. As can be seen in figure 10 (a), random-phase noise is a good approximation to broadband noise, where no dominant frequency appears. We notice in figure 10(b) that the spectrum does not have a single sharp peak at the fundamental frequency, but the energy is distributed in a broad band

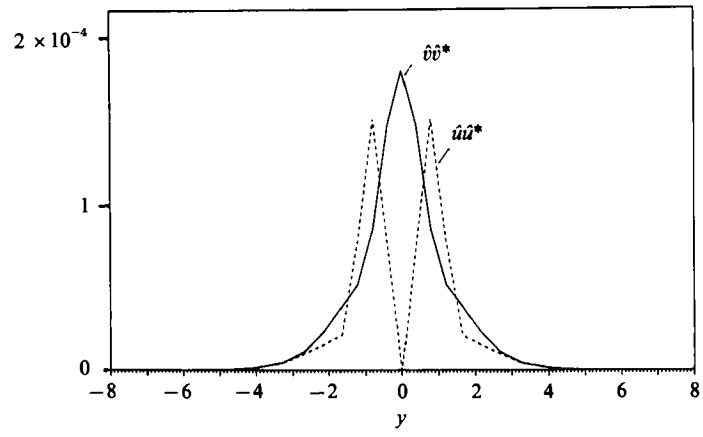

FIGURE 8. Profile of the fundamental mode ($\hat{v}\hat{v}^*$, $\hat{u}\hat{u}^*$) at $x = 25$; Case with low-amplitude random noise.

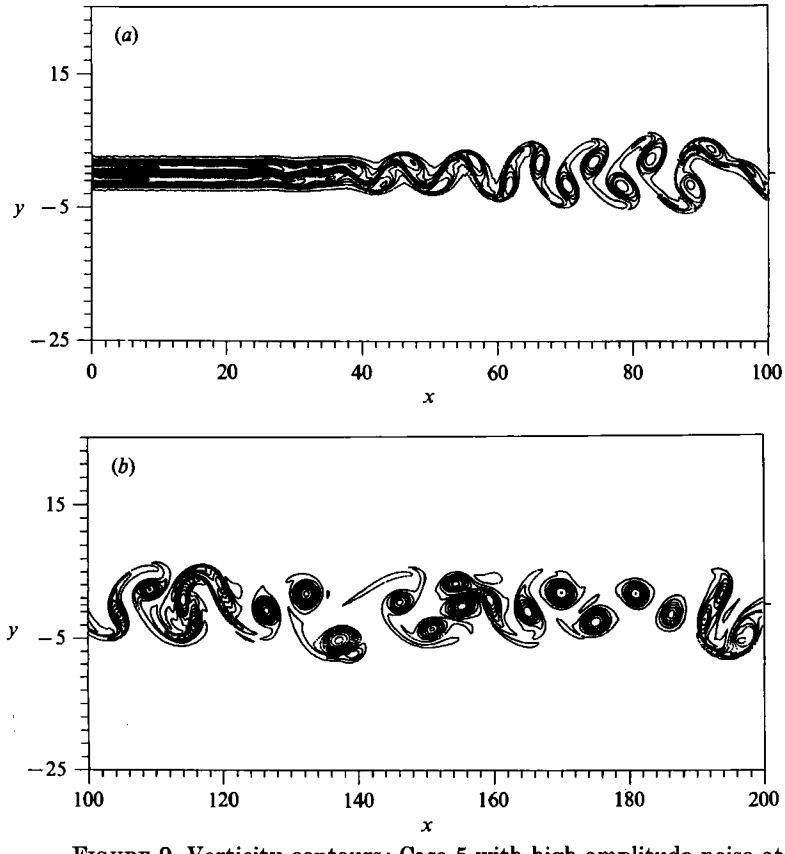

FIGURE 9. Vorticity contours; Case 5 with high-amplitude noise at $Re = 600$ (contour interval: 0.0625 in (*a*), 0.045 in (*b*)).

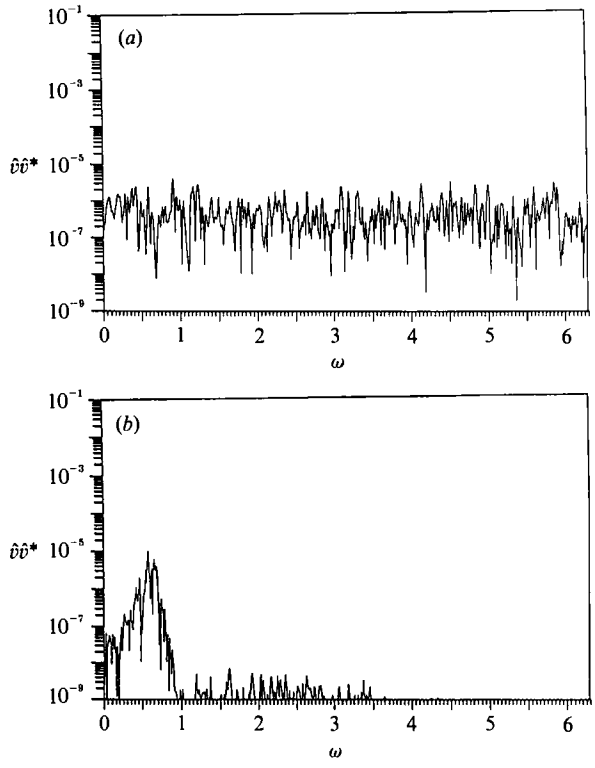

FIGURE 10. Energy spectra of v: Case 5 with high-amplitude noise at $Re = 600$: (a) at inlet plane and $y = 0$, (b) at $x = 25$ and $y = -2.7$.

with frequencies close to the fundamental one. The small variation of the spatial growth rates within this band is responsible for the distorted configuration. In this case, vortex pairing and coupling are part of the wake development.

4.3. *Observation of vortex interactions*

In this subsection, we describe the evolution in time of the vortical structures when the layer is forced by random noise. Experimental measurements at high Reynolds numbers have not detected pairing motions in a plane wake (Robert & Roshko 1985), but earlier low-Reynolds-number flow visualizations by Taneda (1959) suggested that pairing plays a role in the growth of the wake. In our simulation with a fundamental and its subharmonic we did not detect pairing in the length of the domain considered. However, we believe that we can detect (see figure 6) the early stages of pairing and that we would have detected pairing if our computational domain was longer. There is more convincing evidence of the presence of pairing in a forced layer in the time-developing simulations of Aref & Siggia (1981) and Chen, Cantwell & Mansour (1990). In addition to detecting pairing in the forced layer, Aref & Siggia (1981) detected pairing when they allowed the numerical errors to accumulate in time and trigger the instability (presumably emulating random forcing). Figure 11 (a–f) shows the time evolution of the vortical structures when we force the inlet with random noise. The plus-sign vortices have been identified as 1, 2, 3, 6, and 7, and the minus-sign vortices identified as 4, 5, 8, and 9. These vortices change their relative locations in the following snapshots. Figures 11 (b) and 11 (c) show that the

plus-sign vortices 2 and 3, and the minus-sign vortices 4 and 5, start pairing and that vortex 1 is pushed out downstream. Figure 11(*d*) shows that vortices 4 and 5 have paired, while vortices 2 and 3 are still in the processes of merging. Upstream of these vortices, vortices 8 and 9 are also pairing as can be seen in figure 11(*c–e*). After the amalgamation of vortices 8 and 9, vortices 7 and 8 become a vortex couple shown in figure 11(*f*), which is similar to the couples reported in the thin liquid film experiments by Couder & Basdevant (1986). These observations are very similar to those of Aref & Siggia (1981) and seem to be strictly a two-dimensional phenomenon. The experiments in soap films emulate two-dimensional flows, and it seems unlikely that coupling of vortices can occur in three-dimensional wakes. Vortex stretching and viscosity will prevent the coupling from surviving as in two-dimensional flows.

5. Time-averaged statistics

In the previous section we have shown that the development of the structures in the wake is sensitive to inlet forcing. This sensitivity motivates various experimental studies on flow control of wakes. From a practical point of view, control might be desired for both the instantaneous and the averaged field. In this section we study the effects of the different forcing on the development of the mean velocity profiles and the Reynolds stresses. The length of the averaging interval is 600 time units.

5.1. *Velocity profiles*

Figure 12 shows the development of the mean velocity profiles at various x-locations for Case 1 at $Re = 600$. We find that the mean velocity at the edge of the wake exceeds the free-stream velocity at around $x = 100$, which is consistent with the measurements of the wake forced with a sound of single frequency (Sato & Saito 1975). Figure 13 shows the development of the velocity at the wake centre U_c/U_∞. We have also plotted on this figure the development of the half-value width $b_{\frac{1}{2}}$ of the mean profile together with the experimental data of Sato & Saito (1975). The origin of the abscissa in our case is the inlet plane, while the trailing edge is used in experimental measurements. Direct comparison is therefore difficult. The velocity U_c/U_∞ at the wake centre increases from $x = 0$ to $x = 65$ and then decreases to $x = 115$. The half-value width $b_{\frac{1}{2}}$ increases rapidly and reaches a maximum near $x = 45$. The general trends of the streamwise variations of U_c/U_∞ and b are the same as measured by Sato & Onda (1970). The maximum value of b is smaller than that of the measurement. For the relatively low Reynolds number $Re = 200$, the distributions of U_c/U_∞ and b show a gradual increase. The maximum values are about the same as those of $Re = 600$ but their x-locations are shifted downstream. In Case 2 and Case 3, where the amplitudes of the fundamental mode and its subharmonics are 0.01, the distributions of b are slightly larger than that of Case 1. In Case 5, U_c/U_∞ and b are similar to those of Case 1, but the x-locations of the respective peaks are shifted downstream. As can be seen by comparing figures 3 and 9, the vortex street in Case 5 is generated further downstream than in Case 1.

5.2. *Velocity fluctuations*

Distributions of $\overline{u^2}$, $\overline{v^2}$ and $\overline{uv}$ for Case 1 at $Re = 600$ are shown in figure 14, where the scales of the fluctuation components in figures 14(*a*), 14(*b*) and 14(*c*) are the same. The u-fluctuation grows rapidly at small x. The maximum value of $\overline{u^2}$ is located at $x = 35$. The vortical structures are created around this location (see figure 3). We notice from figures 3 and 14(*a*) that the y-locations of the two peaks in $\overline{u^2}$ correspond

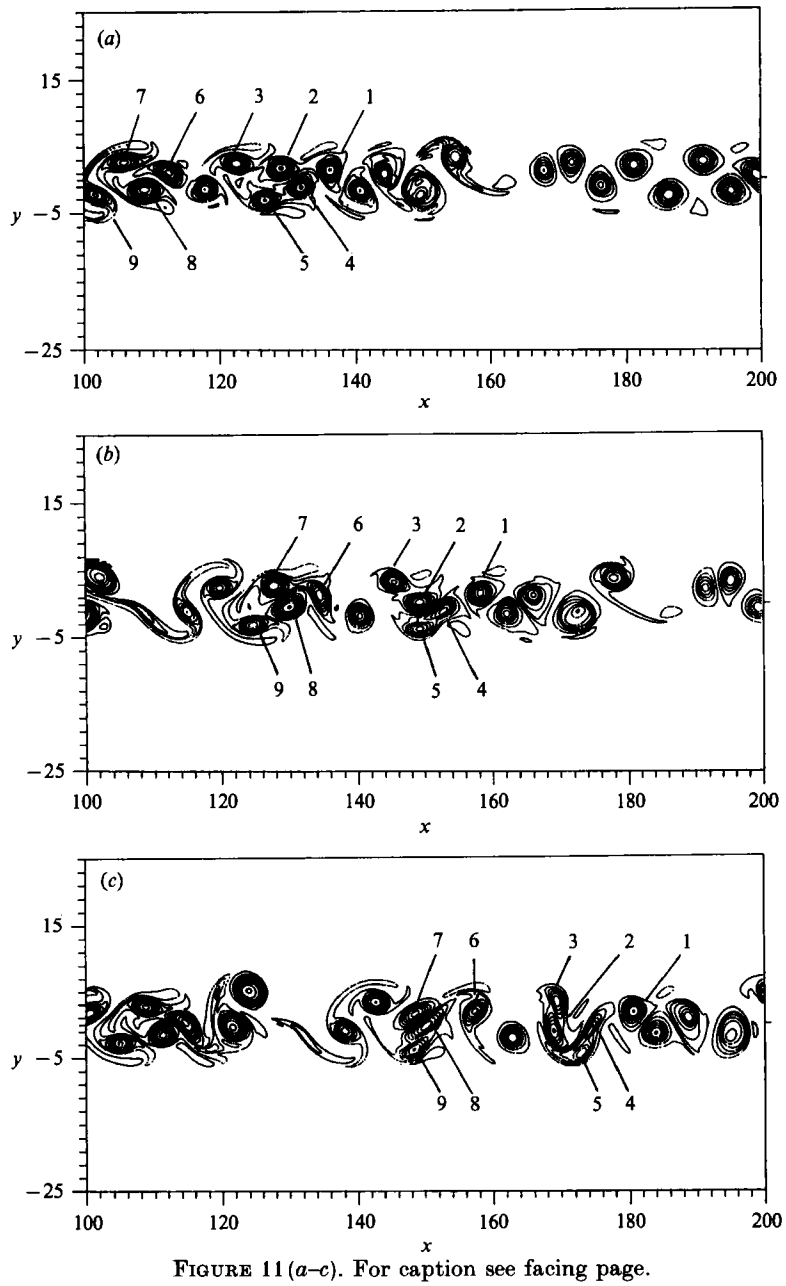

FIGURE 11 (*a–c*). For caption see facing page.

to the outside edges of the vortices. Figure 14(*c*) shows that $\overline{uv}$ changes sign around $x = 50$, which agrees with the measurements by Sato & Onda (1970). At $Re = 200$, the u-fluctuation grows rapidly at small x, but the maximum value of $\overline{u^2}$ is smaller than that at $Re = 600$. We conclude that the maximum value of $\overline{u^2}$ increases as the Reynolds number increases. Figure 15 shows the streamwise variations of the maximum root-mean-square value of the u-fluctuation as a function of x for Case 1. The distribution has two peaks, which is consistent with the measurement of the forced wake of Sato & Saito (1975). The maximum peak value of the numerical result

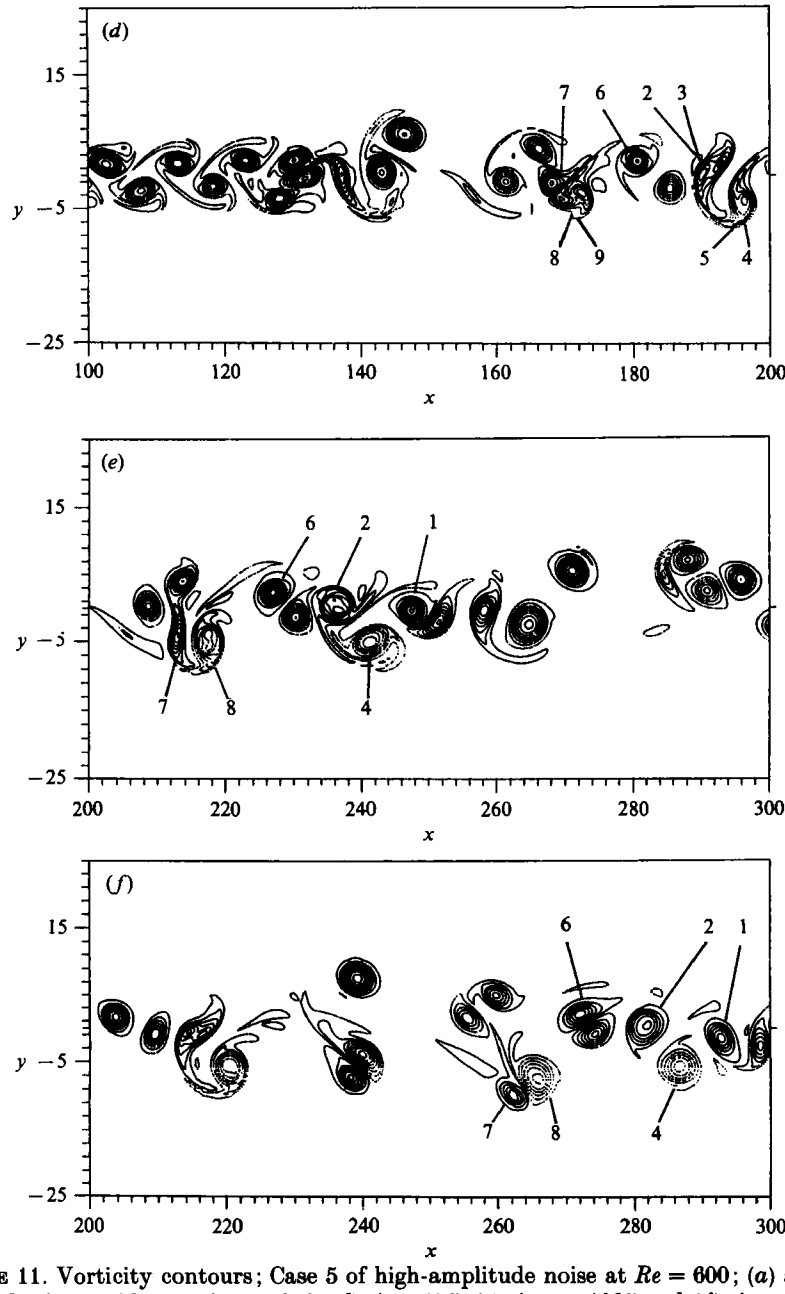

FIGURE 11. Vorticity contours; Case 5 of high-amplitude noise at $Re = 600$; (*a*) at time = 900, (*b*) time = 925, (*c*) time = 950, (*d*) time 975, (*e*) time = 1025 and (*f*) time = 1075.

is smaller than that of the measurements. The reason is that the Reynolds number of the simulation is smaller than that of the experiment by Sato & Saito (1975), where the Reynolds number is about 850. The u-fluctuations in the case of random forcing (Case 5) are different from those with periodic forcing (see figure 16*a*). The scales of figure 14 and figure 16 are the same. The profile at about $x = 40$ has symmetric peaks, though the magnitude is smaller than in Case 1. The maximum magnitude (0.1) of the root-mean square value of the u-fluctuation is close to the experiments (0.105) in

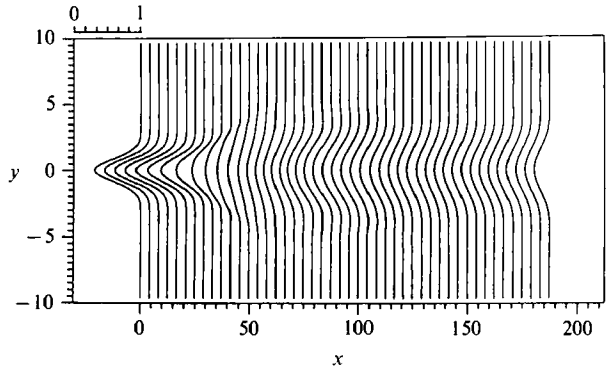

FIGURE 12. Mean velocity profiles; Case 1 at $Re = 600$.

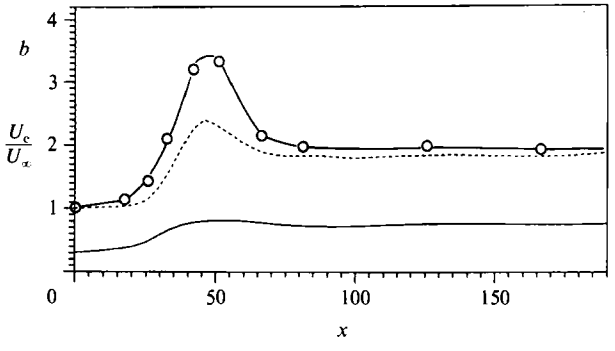

FIGURE 13. Development of the mean velocity at the wake centre U_c/U_∞ (solid line) and of the half-value width b (dotted line); Case 1 at $Re = 600$. The circles are experimental measurements of the half-width by Sato & Saito (1975).

natural transition. The distributions of $\overline{u^2}$ for large x are different from those of Case 1. In this case, the two-peaks profile of $\overline{u^2}$ does not exist. Some profiles at large x have a maximum around the wake centre, which is consistent with the experimental measurements of natural transition. We observe in the vorticity contours of the wake forced with random noise that the vortices pass near the wake centre. In both Cases 1 and 5, the distributions of $\overline{v^2}$ have peaks at the wake centre upstream of the locations where the alternate-signed vortices appear, as shown in figures 14(b) and 16(b). In Case 1 we notice that $\overline{v^2}$ at $x = 70$ has the characteristic two-peak distribution. Further downstream, the two peaks gradually flatten. In Case 5, the distributions of $\overline{v^2}$ at large x are different from those of Case 1, which is related to the relaxation of coherency in the former case. Figure 16(c) shows the distributions of the $\overline{uv}$ fluctuation of Case 5. We notice that this distribution also changes sign at around the location where the vortex street appears. However, in this case the magnitude of the intensity is smaller than in Case 1. These results show that the specific profiles of $\overline{u^2}$, $\overline{v^2}$ and $\overline{uv}$ are determined by the vortical structures.

6. Growth of the fundamental mode, subharmonics and randomness

We point out that for the Gaussian profile and Reynolds numbers considered in this study, a steady laminar-wake solution is obtained when the forcing is stopped. Consequently, the wake in this case is convectively unstable. We know that the

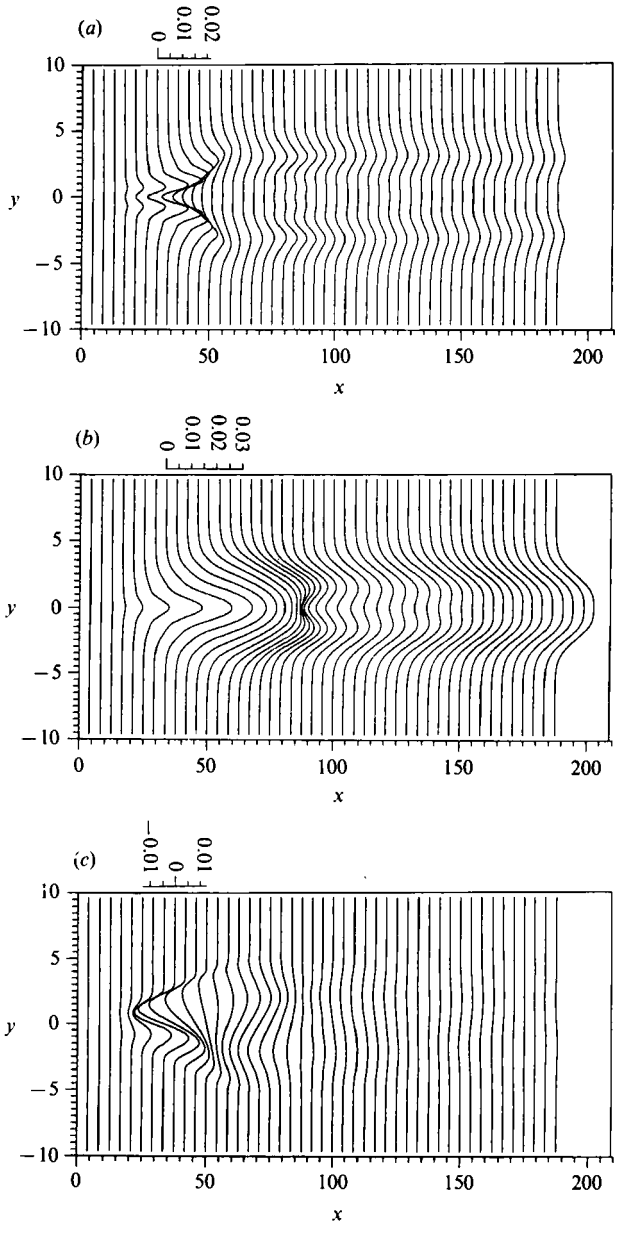

FIGURE 14. Profiles of the Reynolds stresses; Case 1 at $Re = 600$: (*a*) $\overline{u^2}$, (*b*) $\overline{v^2}$, (*c*) $\overline{uv}$.

spatial growth of the fundamental mode is responsible for the generation of the vortex street in the wake. In this section, we will examine the spatial growth of modes with various frequencies and discuss their nonlinear interactions.

We first examine the development of the modes when the layer is forced by a single frequency. Figures 17 (*a*) and 17 (*b*) show that the streamwise distribution for Case 1 at $Re = 200$ of the fundamental and the first harmonic component of u at $y = 2.2$ and $y = 0$, respectively. We notice in figure 17 (*a*) that the peak of the fundamental component is located near $x = 55$, where the vortices appear. We also notice in figure 17 (*b*) that the distribution of the first harmonic peaks earlier, near $x = 45$. At the

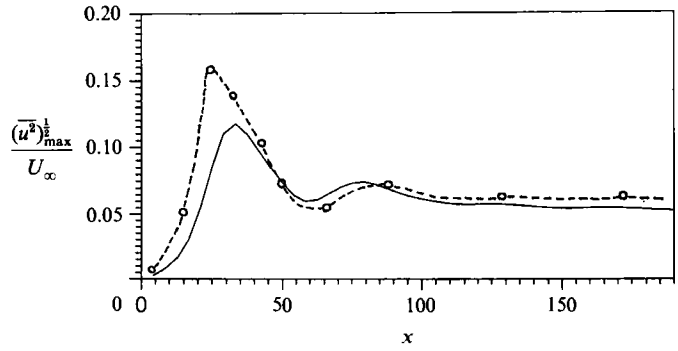

FIGURE 15. Development of the maximum $(\overline{u^2})^{\frac{1}{2}}$; Case 1 at $Re = 600$: circles are experimental measurements by Sato & Saito (1975).

wake centre, the fundamental component of u is zero while the first harmonic component is not zero. This agrees with the experimental results of Sato & Kuriki (1961).

Adding two subharmonics to a fundamental frequency (Case 3 at $Re = 200$), figures 18(a) and 18(b) show the distribution of the fundamental, and first and second subharmonic components of u at $y = 2.2$ and $y = 0$. We find a peak near $y = 2.2$ in the cross-stream u^2 profile of the first subharmonic component further downstream at $x = 125$. Figure 18(a) indicates that the fundamental mode grows faster than its two subharmonics and that the first subharmonic grows after the saturation of the fundamental. The location where the fundamental peaks is the same as for Case 1, but the amplitude is slightly smaller in Case 3. We notice in figure 18(b) that the distribution of the first subharmonic and the first harmonic at $y = 0$ have peaks at about $x = 45$. The vorticity contours (figure 6) show that the first peak in both first subharmonic and first harmonic components at the wake centre occur at the same location as where the alternate-signed vortices appear. At large x, the first subharmonic component of u starts to grow again, which appears to lead to the early stages of pairing.

When the inlet is forced with low-amplitude (0.00001) random-phase noise (Case 5), the fundamental mode grows faster than the others in the linear region. Figure 19(a) shows the spectrum of v^2 at $x = 50$ and $y = -0.8$, which is close to an inflexion point of the mean profile. The spectrum has a sharp peak at the fundamental frequency with a band around it. The bands around the fundamental and its harmonics correspond to the 'humps' of Sato & Saito (1975). Figure 19(b) shows that the spectrum of u^2 also has a peak at the fundamental mode similar to that of v^2. The cross-stream distribution of the fundamental component has a profile similar to that of Case 1, as shown in figure 8, though the magnitudes in this case are smaller. The fundamental component continues to grow to about $x = 90$, where the vortex street appears. The spectra at $x = 75$ (see figure 19c, d) show the dominance of the fundamental. We can see in figure 18(f) that the growth of the fundamental component of u at $y = -1.7$ begins to saturate after the appearance of the vortex street. On the other hand, the amplitudes of the frequency components around the first subharmonic are small up to $x = 100$. We notice in figure 19(g, h) that the amplitude of the first subharmonic component gradually increases after the rapid decrease of the fundamental component. The amplitude around the second subharmonic frequency grows faster than the amplitude near the first subharmonic,

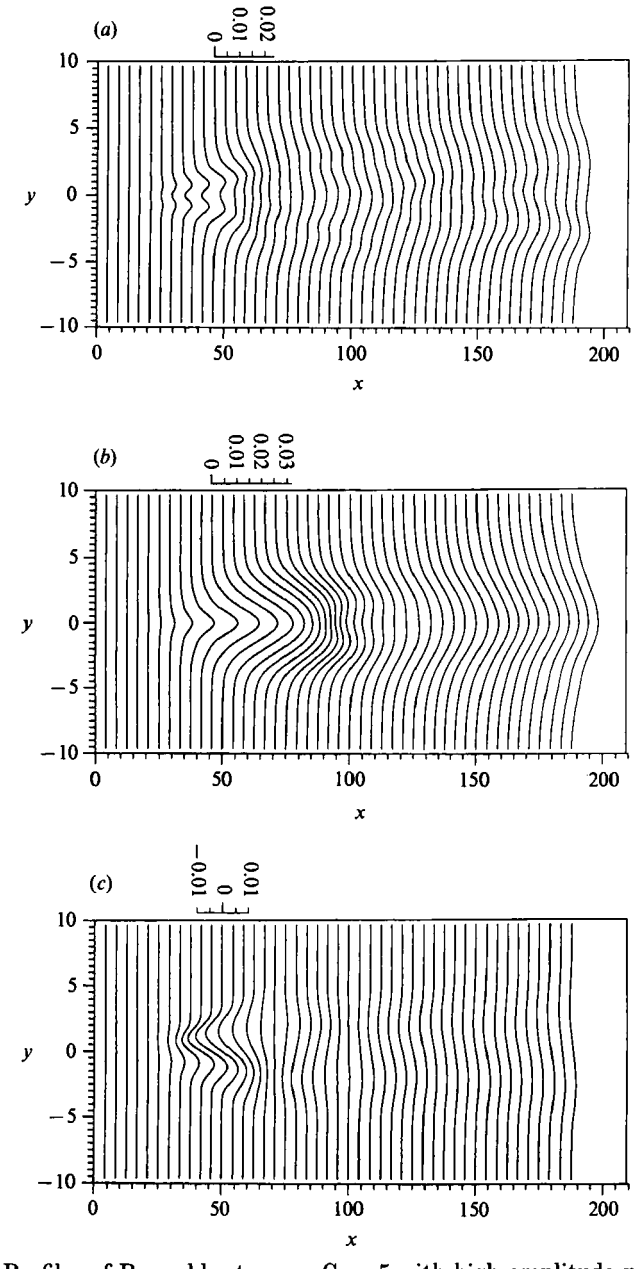

FIGURE 16. Profiles of Reynolds stresses; Case 5 with high-amplitude noise at $Re = 600$: (*a*) $\overline{u^2}$, (*b*) $\overline{v^2}$, (*c*) $\overline{uv}$.

as shown in figure 19. The cross-stream distribution of the energy in the second subharmonic is shown in figure 20 ($\omega = 0.152$). We find a peak in the u^2 profile at the wake centre in contrast to the profile of the fundamental mode. In this case we observe the formation of alternate-signed vortices around $x = 75$. The spectra at $x = 75$ in figures 19(*c*, *d*) show higher harmonics with bands around them. Further downstream at $x = 100$ and 150, after the fundamental mode saturates, the bands broaden and the amplitude at the fundamental frequency starts to decrease. The

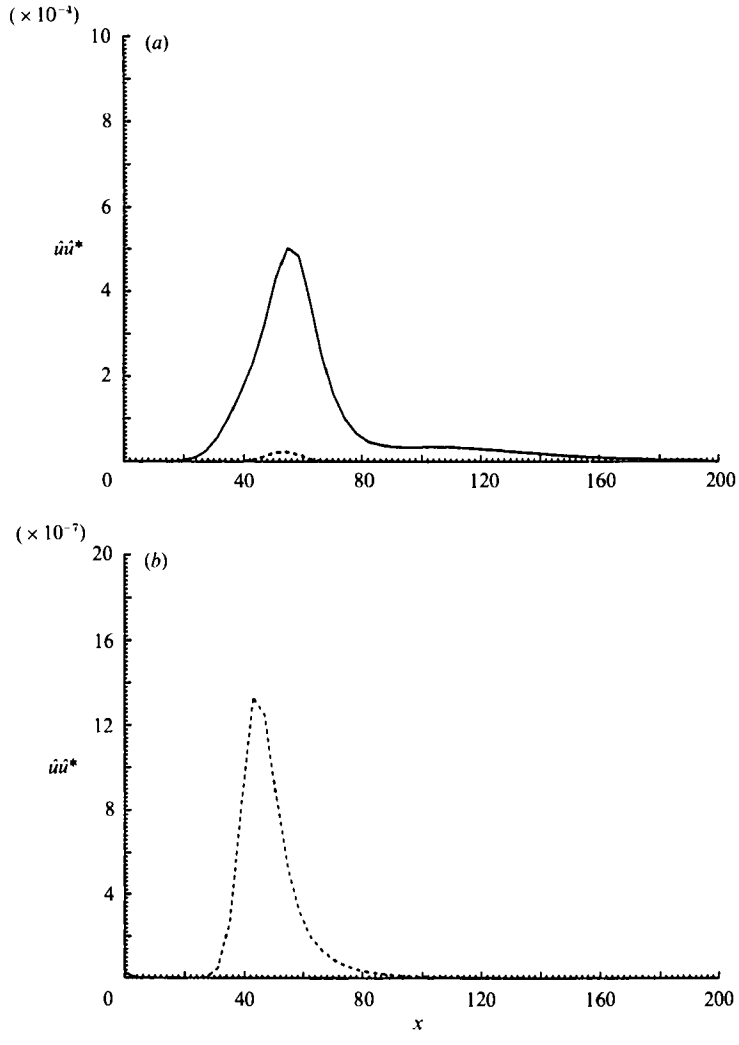

FIGURE 17. Development of the fundamental mode (solid line) and its first harmonic (dashed line) with downstream distance; Case 1 at $Re = 200$: (*a*) $y = 2.2$, (*b*) $y = 0$.

amplitude at frequencies lower than the fundamental grows gradually as shown in figures 19(*e–h*). We notice in figures 19(*g*, *h*) that the amplitude of the sharp peak at the fundamental frequency decreases with x for both components. The fundamental component of u becomes indistinguishable from the noise, while v maintains a sharp peak at the fundamental frequency. These observations are consistent with experimental measurements.

In Case 4 we introduced at the inlet plane a fundamental mode and a random-phase noise of small amplitude. The amplitude of the fundamental mode is 0.01 and that of the random-phase noise is 0.0005. Figures 21(*a*), 21(*b*) and 21(*c*) show the spectra of the v-component at $x = 0$, 75, and 150, respectively. We notice the growth of a band around the fundamental mode as we move downstream. As the higher harmonics develop, a band also develops around them (see figure 21). On the other hand the noise at frequencies lower than the fundamental does not grow as much as it does in Case 5 at $x = 150$. This is an indication that the presence of the

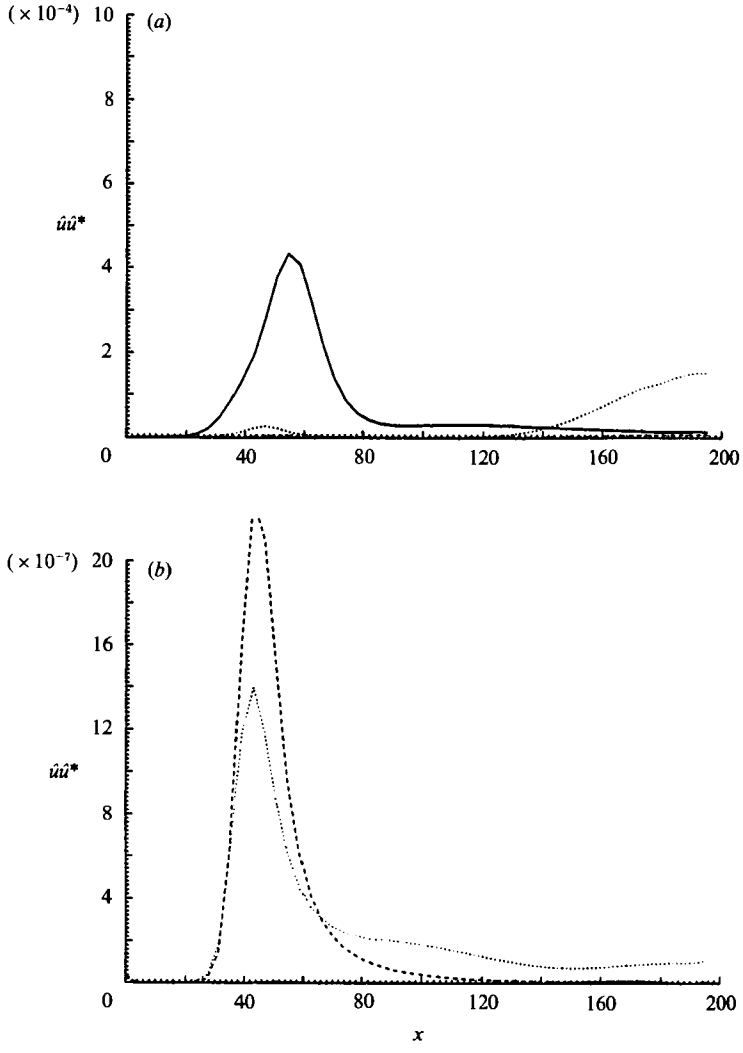

FIGURE 18. Development of the fundamental mode and its first two subharmonics; Case 3 at $Re = 200$: (*a*) $y = 2.2$ (solid line: fundamental, dotted line: first subharmonic, dashed line: second subharmonic), (*b*) $y = 0$ (dotted line: first subharmonic, dashed line: first harmonic).

fundamental has suppressed the growth of the noise. We have investigated spatial distributions of the fundamental and other frequency components. Figures 22 (*a*) and 22 (*b*) show the cross-stream distribution of the fundamental component at $x = 50$ and 150, respectively. The profiles of u^2 and v^2 are similar to those of Case 1. In both Cases 1 and 4, and after the fundamental saturates, the profiles of u^2 and v^2 spread out only slightly, even by $x = 150$. The distributions of the second subharmonic frequency are shown in figure 22 (*c*, *d*). The profile of u^2 has one peak at the wake centre at $x = 50$ and two peaks at $x = 150$. The magnitude of u^2 is larger than that of v^2. Figures 22 (*e*), 22 (*f*), 22 (*g*), and 22 (*h*) show the cross-stream distributions of u^2 and v^2 at $x = 150$, for frequencies corresponding to 0.704, 0.508, 0.408, and 0.102, respectively. The distribution of the fundamental mode is symmetric, as shown in figure 22 (*a*). The profile of u^2 has two peaks with zeros off the centreline, which is consistent with the measurement of Sato & Kuriki (1961). Figure 22 (*e*, *f*) shows the profiles around the

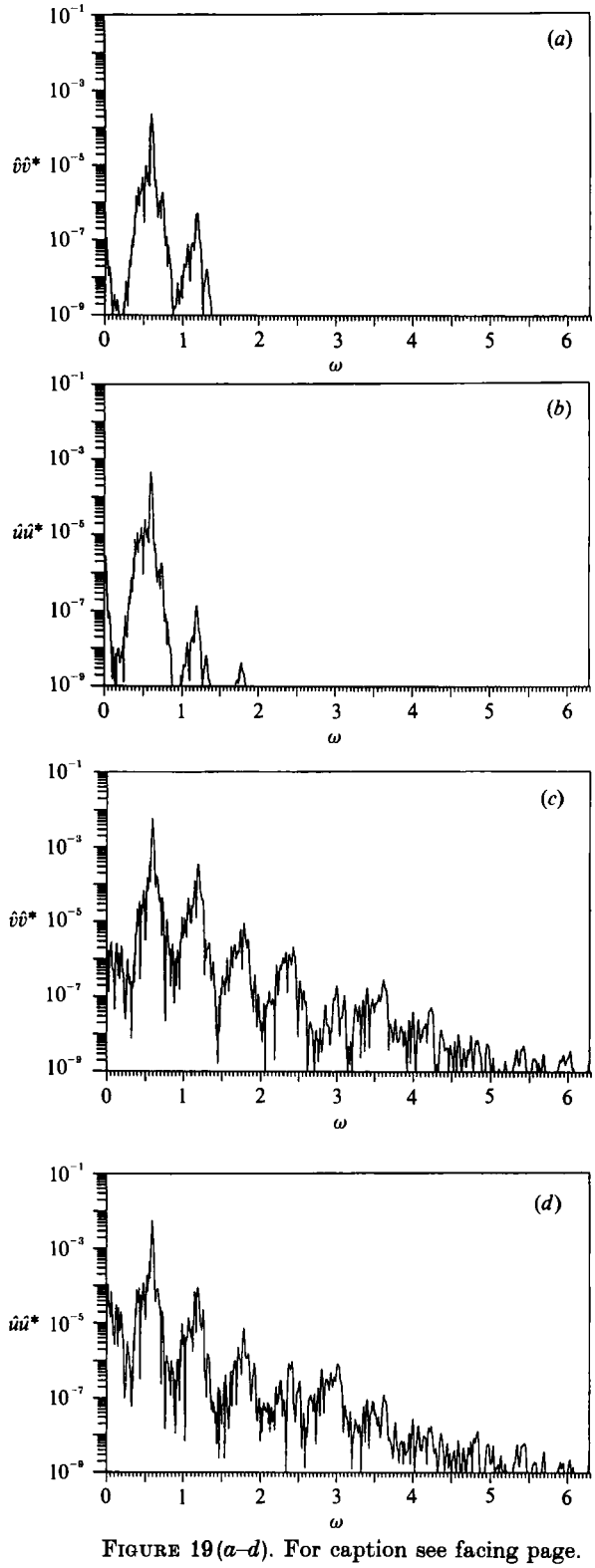

FIGURE 19(*a–d*). For caption see facing page.

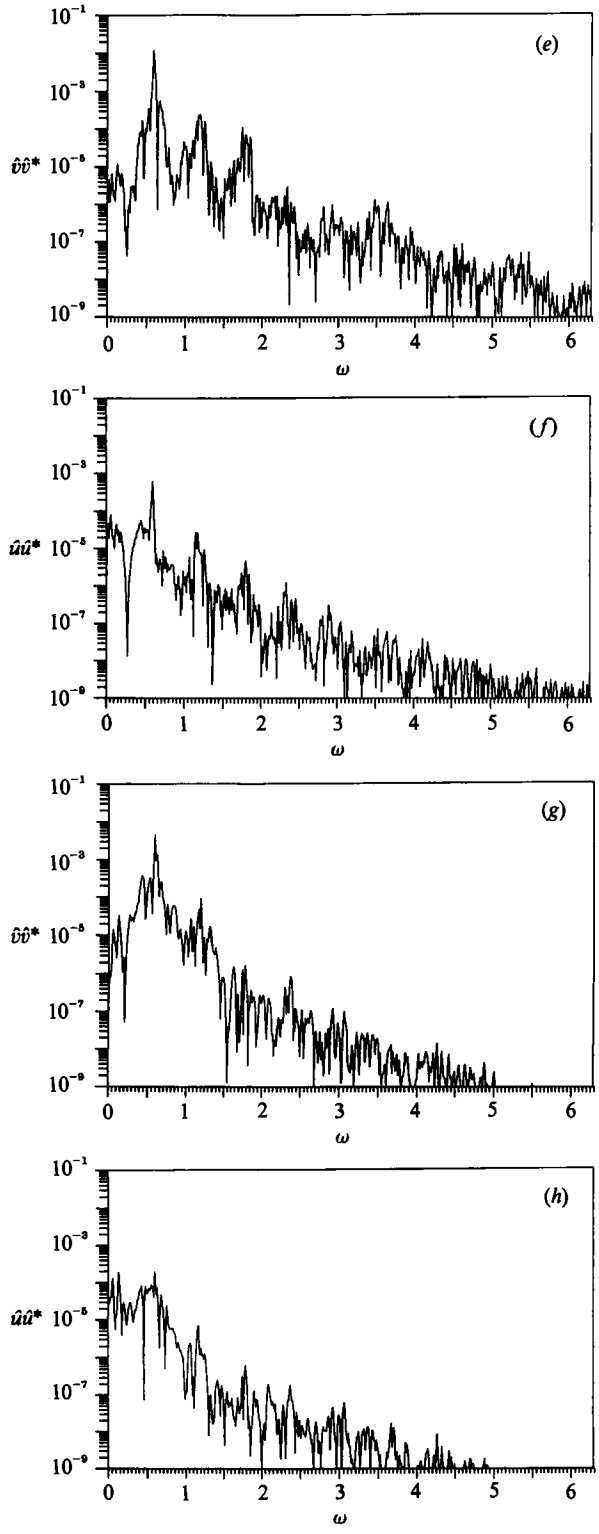

FIGURE 19. Energy spectra of u and v; Case 5 with low-amplitude noise at $Re = 600$: (a, b) $x = 50$, $y = -0.8$; (c, d) $x = 75$, $y = -1.7$; (e, f) $x = 100$, $y = -1.7$; (g, h) $x = 150$, $y = -2.1$.

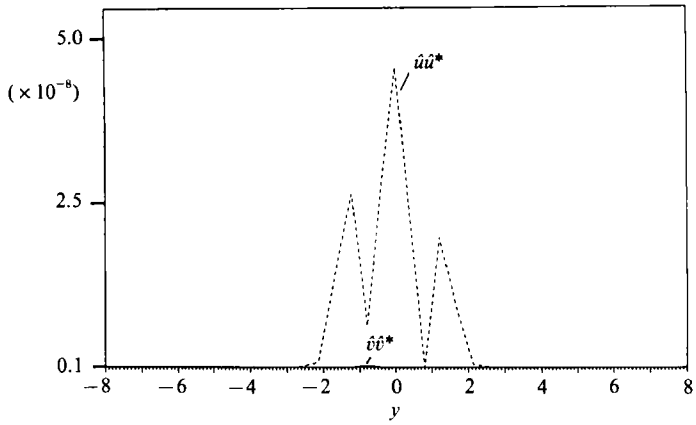

FIGURE 20. Profile of the second subharmonic ($\hat{v}\hat{v}^*$, $\hat{u}\hat{u}^*$) at $x = 50$; Case 5 with low-amplitude noise at $Re = 600$.

fundamental mode. We notice that these shapes are similar to those of the fundamental mode, while the shapes of the distributions at frequencies lower than the fundamental are different from those of the fundamental mode, as shown in figure 22(*h*). Though the growth of this noise is suppressed strongly by the fundamental mode, the noise around the fundamental mode grows as the intensity of the fundamental mode increases. On the other hand, the subharmonic noise grows gradually after the saturation of the fundamental mode, as shown in figure 21(*c*). The amplitude of the fundamental mode at the inlet plane is so high that the flow can be locked, which is similar to the experimental results of Gharib & Williams-Stuber (1989).

In Case 5, with a noise amplitude of 0.01, the spectrum around the fundamental mode develops as we move downstream. Figures 10(*b*), 23(*a*), 23(*b*) and 23(*c*) show the spectra of v and u, at $x = 25$ and $y = -2.7$, and at $x = 175$ and $y = -1.7$. We can observe in figures 10(*b*), 23(*a*) that the spectra have a continuous energy band around the fundamental mode but does not have a sharp peak at the fundamental frequency. In this case, the nonlinear interaction between a few modes close to the fundamental frequency are important. We notice in figure 23(*b*,*c*) that the magnitude of the noise, at frequencies lower than the fundamental, is larger than that of the fundamental. Figures 24(*a*) and 24(*b*) show phase diagrams at $x = 25$ and $x = 175$, which are at the same x, y locations as figures 23(*a*) and 23(*c*), respectively. Figure 24(*a*) shows a combination of organized and non-periodic traces, while figure 24(*b*) shows a more chaotic-like trace. This indicates that ordered motion (i.e. the vortex street) is generated and that random motion is suppressed, even though the inlet flow is forced by random noise of large amplitude. After saturation of the growth of the organized motion, the flow becomes increasingly random.

In Case 3, with inlet amplitude forcing at 0.01, no significant modes with magnitudes larger than 10^{-14} exist other than the fundamental and its harmonics and first two subharmonics. On the other hand, when the forcing amplitudes are at 0.00001, a band of frequencies develops downstream of the inlet plane, as shown in figure 25(*a*, *b*). In this case, the spectrum becomes full further downstream. We conjecture that at this amplitude, very weak feedback between the outflow and inflow boundaries is able to compete linearly with the forced perturbation. At higher amplitudes, the forced perturbation suppresses the feedback signal through nonlinear

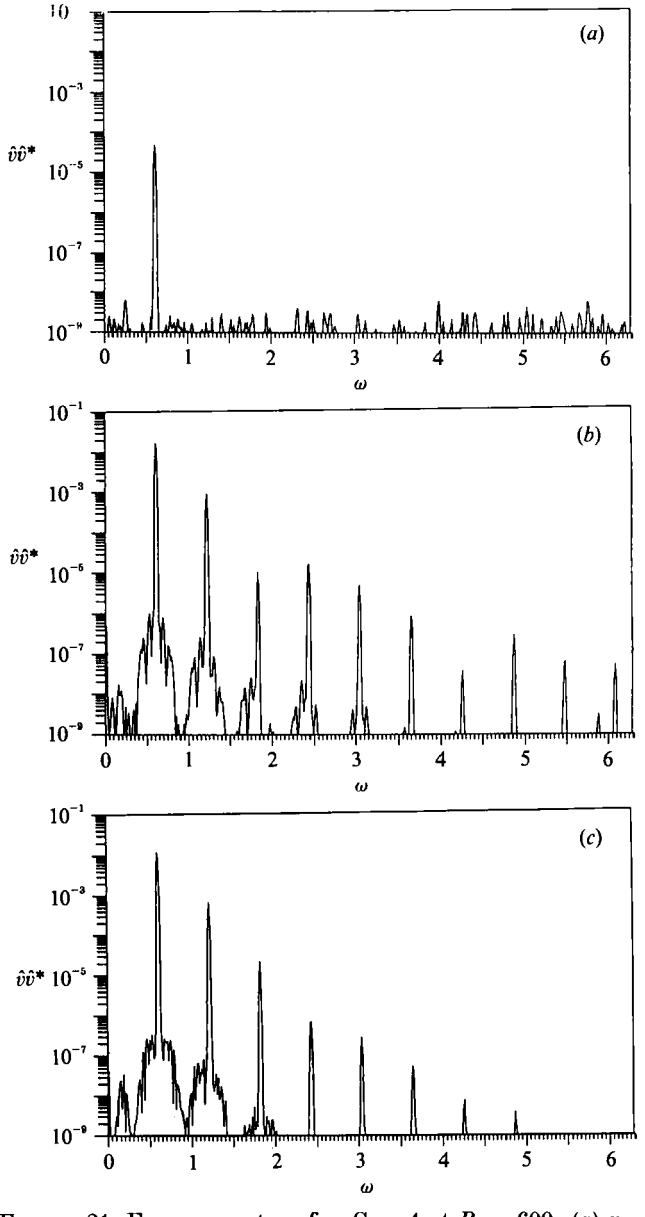

FIGURE 21. Energy spectra of v; Case 4 at $Re = 600$: (*a*) $x = 0$, $y = 0$; (*b*) $x = 75$, $y = -1.7$; (*c*) $x = 150$, $y = -2.1$.

mechanisms to produce 'clean' spectra. Figures 25(*e*) and 25(*f*) show the spectra of v^2 and u^2 at $x = 150$. The spectra show a sharp peak at the fundamental frequency at $x = 150$. Since the magnitude of the fundamental is large and that of the first subharmonic is small at $x = 150$, we observe a vortex street in figure 26 in the range of $100 < x < 200$. Figure 25(*c*, *d*) shows a rapid growth of the fundamental frequency at $x = 50$. At $x = 150$, the spectra of u- and v-fluctuations show a sharp peak at the fundamental frequency with the other modes in the spectrum beginning to have significant energy. Since the magnitude of the fundamental component is much larger

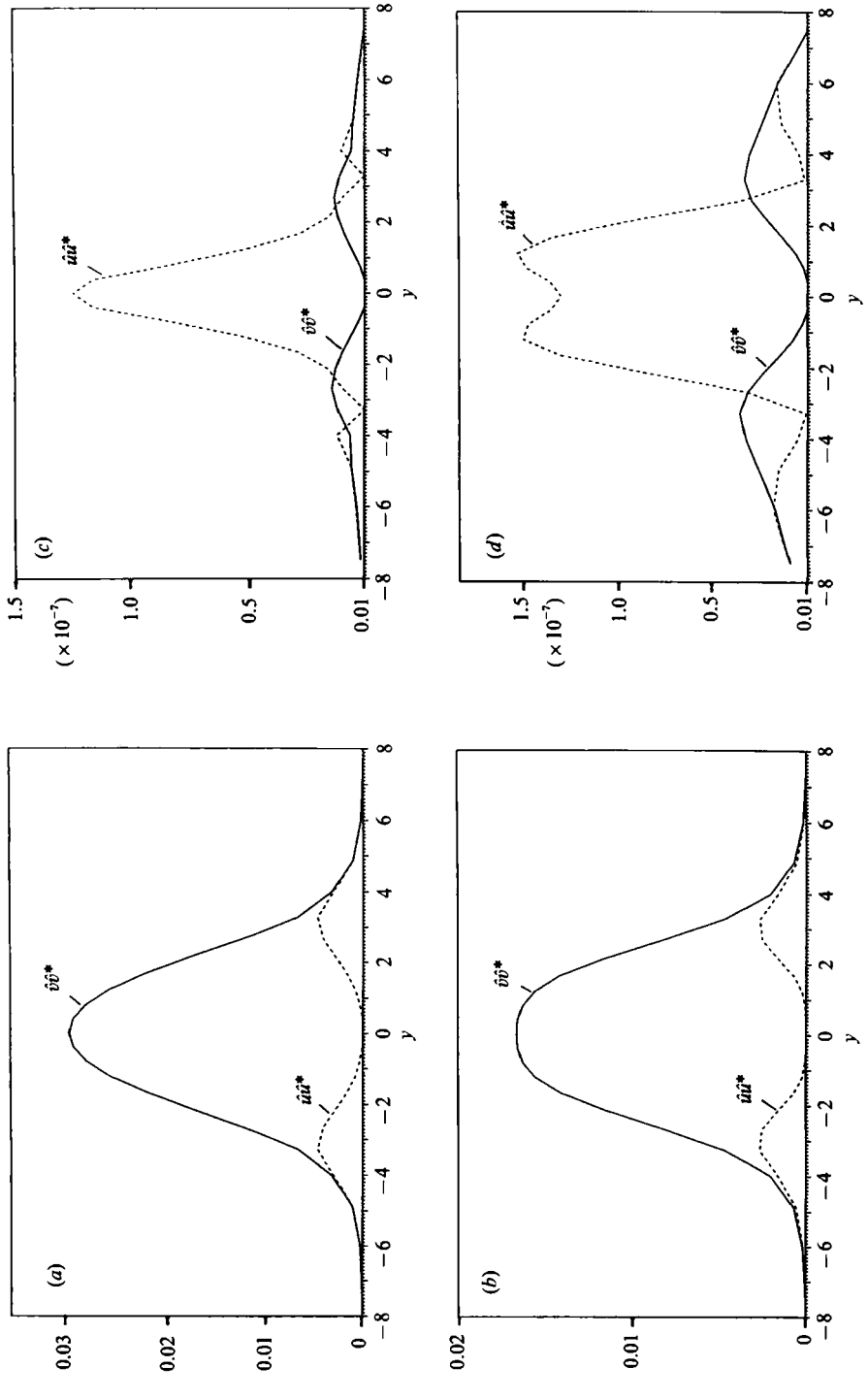
(a)
(b)
(c)
(d)
$\hat{v}\hat{v}^*$
$\hat{u}\hat{u}^*$
y
$(\times 10^{-7})$

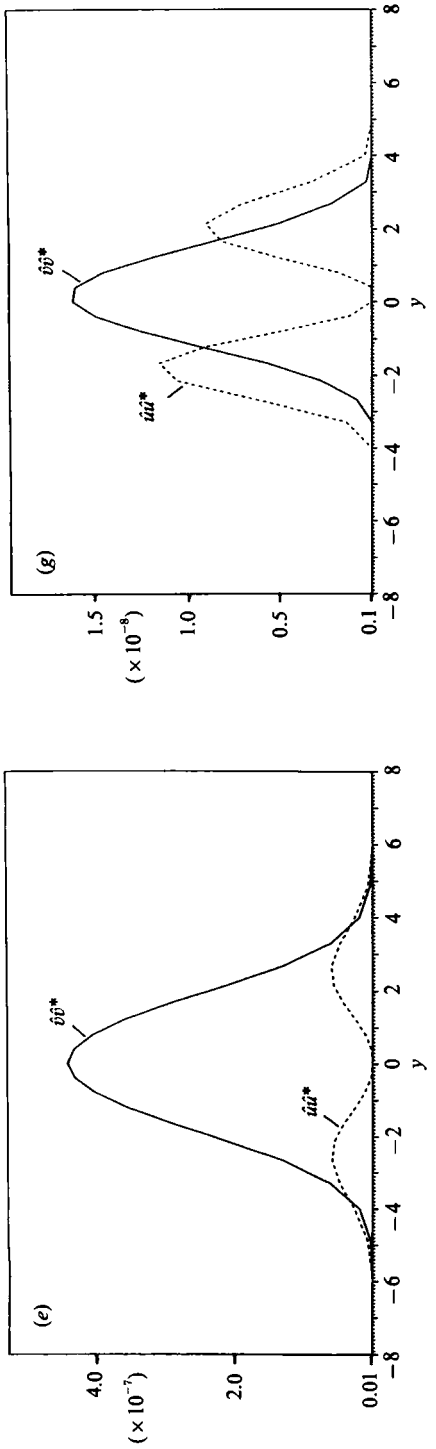

FIGURE 22. Profiles of the fundamental component and other components; Case 4 ($\hat{v}\hat{v}^*$, $\hat{u}\hat{u}^*$): (*a*) fundamental component at $x = 50$, (*b*) fundamental component at $x = 150$, (*c*) second subharmonic at $x = 50$, (*d*) second subharmonic at $x = 150$, (*e*) frequency component $\omega = 0.704$ at $x = 150$, (*f*) frequency component $\omega = 0.508$ at $x = 150$, (*g*) frequency component $\omega = 0.408$ at $x = 150$, (*h*) frequency component $\omega = 0.102$ at $x = 150$.

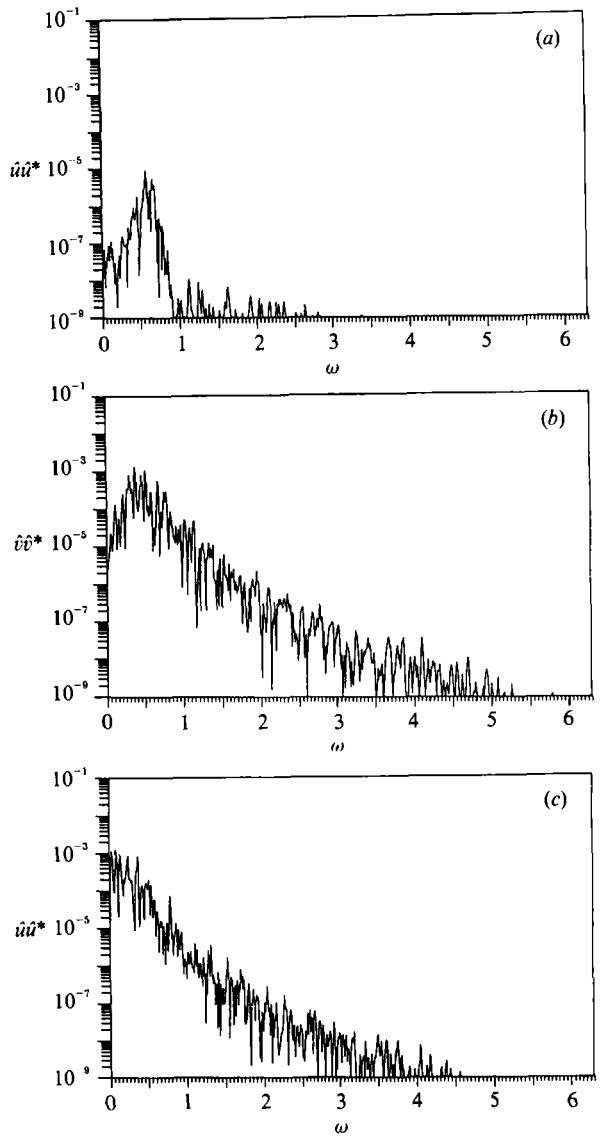

FIGURE 23. Energy spectra of u and v; Case 5 with high amplitude noise: (*a*) $x = 25$, $y = -2.7$; (*b*) $x = 175$, $y = -1.7$; (*c*) $x = 175$, $y = -1.7$.

than other modes, we do not observe in a snapshot of vorticity the existence of a full spectrum.

To summarize, we have found selective spatial amplification of the fundamental mode and spatial amplification of its subharmonics. These are responsible for the appearance of the vortex street and its deformation. When we introduce a fundamental mode and random-phase noise at the inlet plane, where the amplitude of the fundamental mode is high, locking at the fundamental frequency suppresses the growth of low-frequency noise. After saturation of the locking frequency, low-frequency noise grows gradually. On the other hand, with small-amplitude forcing, low frequency noise appears before the appearance of the vortex street, since the fundamental mode at small magnitudes does not lock the flow.

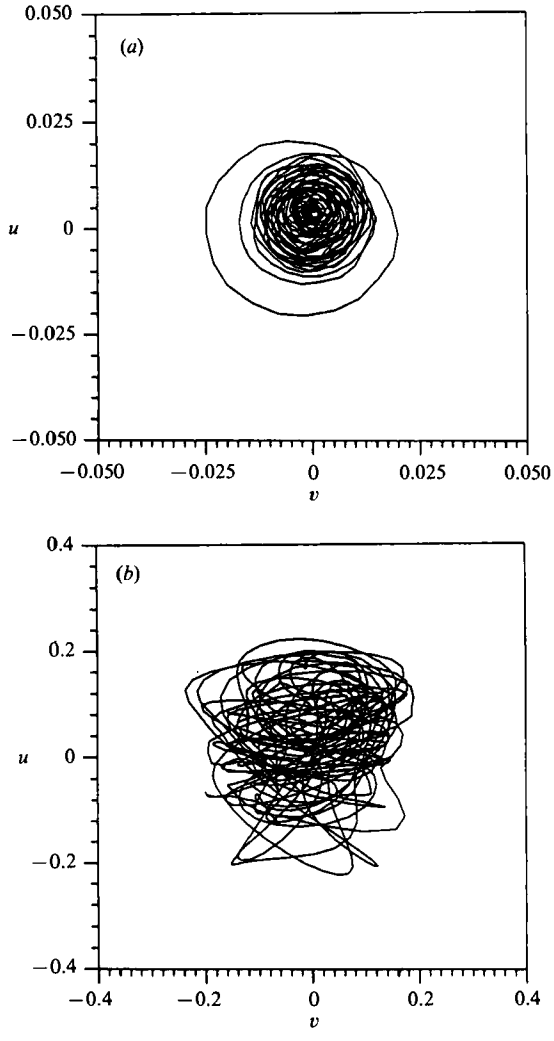

FIGURE 24. Phase diagrams; Case 5 with high-amplitude noise; (*a*) $x = 25$, $y = -2.7$; (*b*) $x = 175$, $y = -1.7$.

7. Absolutely unstable wakes

It is known from parallel flow theory (see Hultgren & Aggarwal 1987) that a Gaussian wake with no reverse flow can have a region of absolute instability. All previous numerical simulations that detect absolute instability considered wakes behind bluff bodies where reverse-flow regions exist. In this section we investigate the case of a wake with no reverse flow. Hultgren & Aggarwal (1987) determined the critical defect parameter and the supercritical Reynolds number that yield absolutely unstable wakes. We used a Gaussian profile at the inlet plane with a deficit of 0.99. A fundamental mode of amplitude 0.0005 was introduced at the inlet plane for one period. The amplitude of the forcing was then set to zero for the rest of the calculation. We investigate the time traces of the oscillation for $Re = 300$ and 700 at x-locations where the mean defects are similar to the critical values reported by Hultgren & Aggarwal (1987). Interpolating from their results we find that the critical

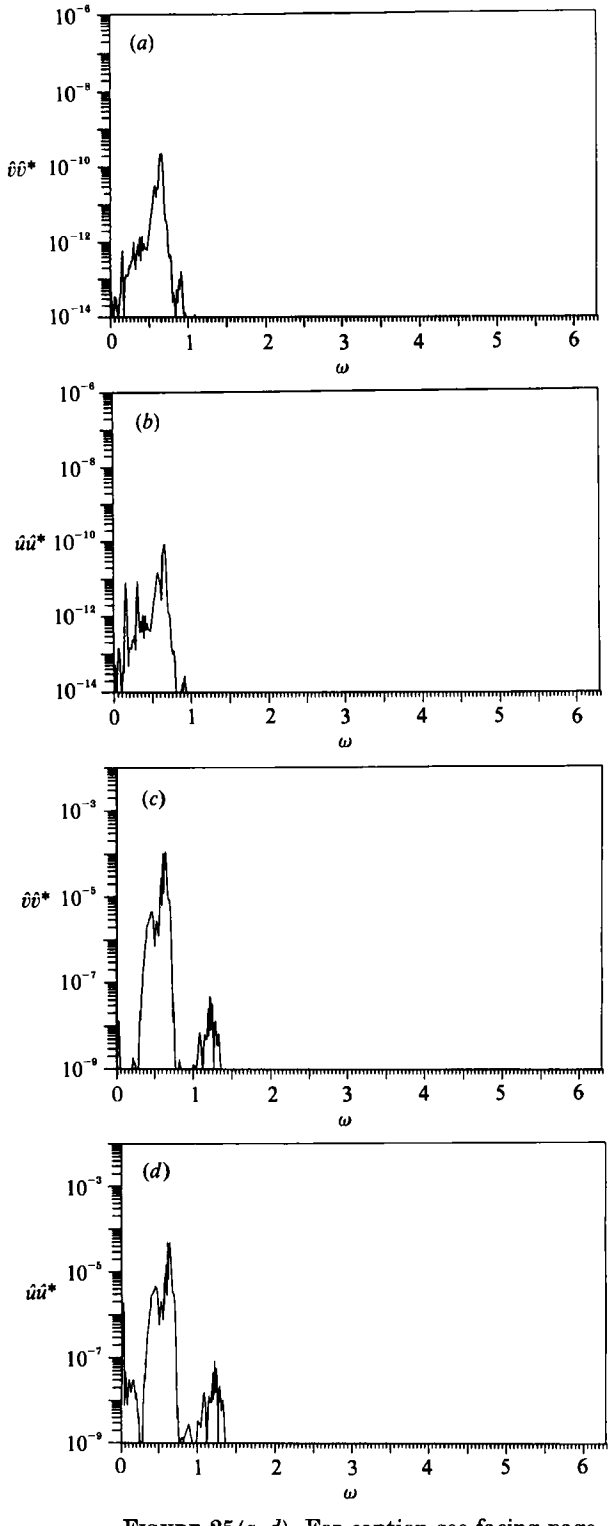

FIGURE 25 (*a–d*). For caption see facing page.

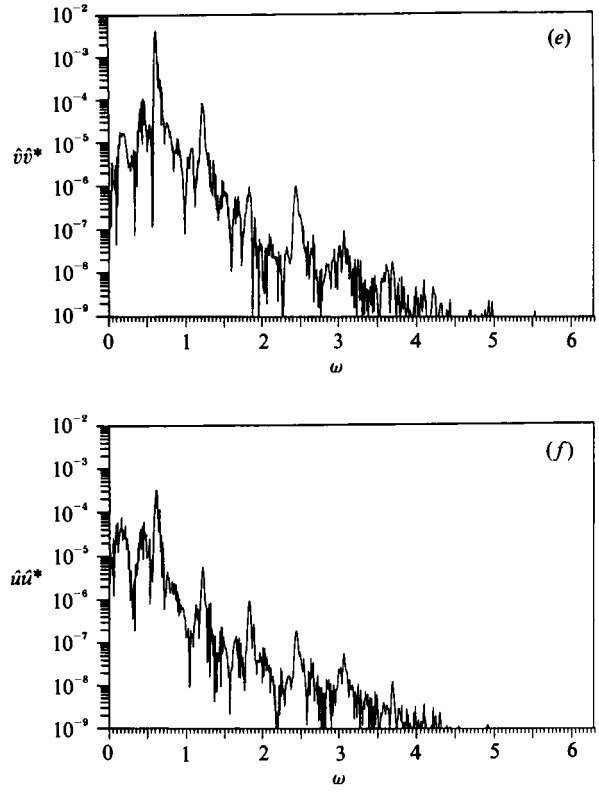

FIGURE 25. Energy spectra of u and v; Case 3 with low-amplitude forcing: (a, b) $x = 2.3$, $y = -0.6$; (c, d) $x = 50$, $y = -0.4$; $(e, f) = 150$, $y = -2.1$.

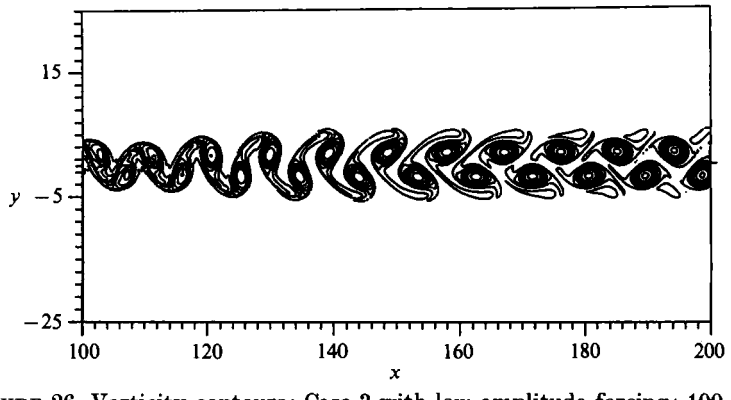

FIGURE 26. Vorticity contours; Case 3 with low-amplitude forcing: $100 < x < 200$ (contour interval: 0.0375).

defect value is 0.955 at $Re = 300$ and is 0.949 at $Re = 700$. At $Re = 300$, the disturbance does not sustain itself (see figure 27*a*), indicating that the layer is globally stable. At $Re = 700$, the time traces show that u and v continue to oscillate after the inlet forcing is stopped (see figure 27*b*). We find that the initial disturbance propagates upstream, as well as downstream, indicating that the layer is globally unstable. Chomaz, Huerre & Redekopp (1988) pointed out that the absolutely unstable region must be larger than a critical length for the onset of global

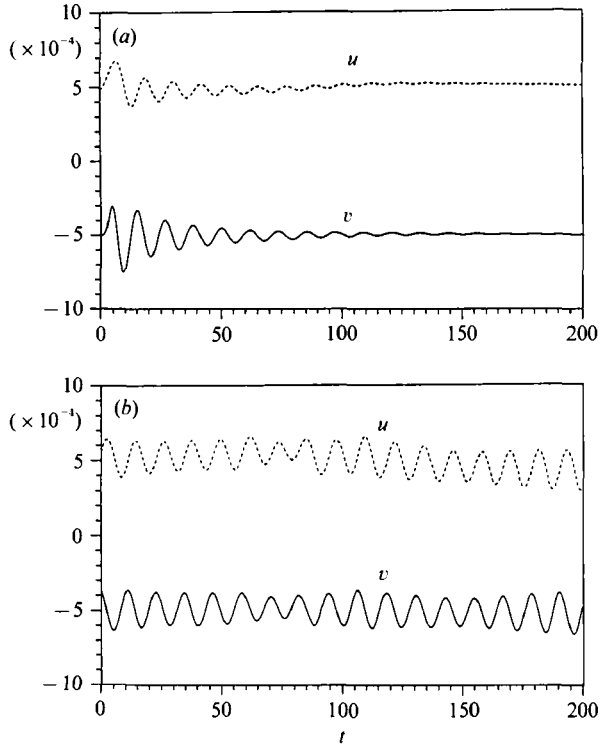

FIGURE 27. Time traces of u and v for large-deficit wake; (a) $x = 2.0$, $y = -0.4$ for $Re = 300$ and (b) $x = 2.7$, $y = -0.6$ for $Re = 700$. The traces of u and v fluctuations are split in positive and negative sides. The plots of initial values of the traces are arbitrary.

instability. The length of the absolutely unstable regions in our calculations is about 2.4 with $Re = 300$ and 3.5, with $Re = 700$. In the latter case the absolutely unstable region is above the critical size. These facts indicate that a wake without a reverse-flow region can be absolutely unstable for sufficiently large Reynolds number and defect.

8. Summary and conclusions

Direct numerical simulations have been used to study the development of forced spatially developing wakes. The flow has been analysed by visualizing the vortical structures through contour plots of vorticity, and by computing the spectra and long-time statistical averages. The computational results compare well with the experimental observations of Sato & Saito (1975). The study of the forced wake through the nonlinear regime indicate the following conclusions:

(i) When only the fundamental mode is forced, a regular vortex street is generated. The fundamental and higher harmonics grow rapidly before the appearance of alternate-signed vortices (vortex street). When a fundamental mode whose magnitude at the inlet plane is much larger than that of external noise is forced, the fundamental mode grows rapidly and suppresses the growth of the other modes. The vortex street that appears downstream will not experience further distortions.

(ii) Two subharmonics forced in addition to a fundamental mode will generate a

distorted vortex street. When the amplitudes of the three modes are large, harmonics of the second subharmonic will grow. For the amplitudes and zero relative phase considered, the energy in the subharmonic at the centreline peaks while the fundamental is saturating. But this growth does not affect the vortical structures. The energy in the first subharmonic grows gradually after the saturation and decay of the fundamental. This growth leads to significant distortion of the vortex street. The effects of relative phase and initial amplitudes were not considered in this work. These effects are known to be important (see for example the work of Meiburg 1987, and Chen *et al.* 1990).

(iii) When the amplitude of the forcing (either random-phase noise or discrete modes) is small, a band around the fundamental frequency is selectively amplified and grows faster than modes at frequencies around the subharmonics. The cross-stream profile of the fundamental mode is quite similar to that of the forced case with a single frequency. Low frequency modes grow after saturation of the fundamental mode.

(iv) When the amplitude of the random-phase noise is large, a band of energy at frequencies close to the fundamental frequency is amplified, but the band is broader than in the small-amplitude case. This will lead to a fuller spectrum and stronger interactions between the vortices downstream. We find vortices of the same sign that pair and vortices of opposite sign that couple. The vortical structures become more randomly distributed as the flow develops.

(v) For an inlet wake deficit of 0.99, the flow is globally unstable at $Re = 700$. The critical size of the absolutely unstable region appears to be about three.

The first author (H.M.) wishes to acknowledge support from the ministry of education exchanging program fund and NASA Ames Research Center. The third author (J.C.B.) acknowledges support from the National Research Council and the Center for Turbulence Research.

REFERENCES

AREF, H. & SIGGIA, E. D. 1981 Evolution and breakdown of a vortex street in two dimensions. *J. Fluid Mech.* **109**, 435–463

BUELL, J. C. 1991 A hybrid numerical method for three-dimensional spatially-developing free-shear flows. *J. Comput. Phys.* **95**, 313–338.

CHEN, J. H., CANTWELL, B. J. & MANSOUR, N. N. 1990 The effect of Mach number on the stability of a plane supersonic wake. *Phys. Fluids* A **2**, 984–1004.

CHOMAZ, J. M., HUERRE, P. & REDEKOPP, L. G. 1988 Bifurcations of local and global modes in spatially developing flows. *Phys. Rev. Lett.* **60**, 25–28.

COMTE, P., LESIEUR, M. & CHOLLET, J. P. 1989 Numerical simulations of turbulent plane shear layers. In *Turbulent Shear Flow 6*, pp. 360–380. Springer.

COUDER, Y. & BASDEVANT, C. 1986 Experimental and numerical study of vortex couples in two-dimensional flow. *J. Fluid Mech.* **173**, 225–251.

DAVIS, R. W. & MOORE, E. F. 1985 A numerical study of vortex merging in mixing layers. *Phys. Fluids* **28**, 1626–1635.

GHARIB, M. & WILLIAMS-STUBER, K. 1989 Experiments on the forced wake of an airfoil. *J. Fluid Mech.* **208**, 225–255.

HANNEMANN, K. & OERTEL, H. 1989 Numerical simulation of the absolutely and convectively unstable wake. *J. Fluid Mech.* **199**, 55–88.

HULTGREN, L. S. & AGGARWAL, A. K. 1987 A note on absolute instability of the Gaussian wake profile. *Phys. Fluids.* **30**, 3383–3387.

KOCH, W. 1985 Local instability characteristics and frequency determination of self-excited wake flows. *J. Sound Vib.* **99**, 53–83.

LELE, S. K. 1991 Compact finite difference schemes with spectral-like resolution. *J. Comput. Phys.* (submitted).

MATTINGLY, G. E. & CRIMINALE, W. O. 1972 The stability of an incompressible two-dimensional wake. *J. Fluid Mech.* **51**, 233–272.

MEIBURG, E. 1987 On the role of subharmonic perturbations in the far wake. *J. Fluid Mech.* **177**, 83–107.

PAPAGEORGIOU, D. T. & SMITH, F. T. 1988 Nonlinear instability of the wake behind a flat plate placed parallel to a uniform stream. *Proc. R. Soc. Lond.* A **419**, 1–28.

PAPAGEORGIOU, D. T. & SMITH, F. T. 1989 Linear instability of the wake behind a flat plate placed parallel to a uniform stream. *J. Fluid Mech.* **208**, 67–89.

ROBERT, A. A. & ROSHKO, A. 1985 Effects of periodic forced mixing in turbulent shear layers and wakes. *AIAA*-85-0570.

SATO, H. & KURIKI, K. 1961 The mechanism of transition in the wake of a thin flat plate placed parallel to a uniform flow. *J. Fluid Mech.* **11**, 321–352.

SATO, H. & ONDA, Y. 1970 Detailed measurements in the transition region of a two-dimensional wake. *Inst. Space & Aero. Sci., Univ. Tokyo, Rep.* 453, pp. 317–377.

SATO, H. & SAITO, H. 1975 Fine-structure of energy spectra of velocity fluctuations in the transition region of a two-dimensional wake. *J. Fluid Mech.* **67**, 539–559.

SATO, H. & SAITO, H. 1978 Artificial control of the laminar turbulent transition of a two dimensional wake by external sound. *J. Fluid Mech.* **84**, 657–672.

TANEDA, S. 1959 Downstream development of the wakes behind cylinders. *J. Phys. Soc. Japan* **14**, 843–848.

WRAY, A. A. 1991 Very low storage time-advancement schemes. *J. Comput. Phys.* (submitted)

ZABUSKY, N. J. & DEEM, G. S. 1971 Dynamical evolution of two dimensional unstable shear flow. *J. Fluid Mech.* **47**, 353–379.